



AMERICAN METEOROLOGICAL SOCIETY

Bulletin of the American Meteorological Society

EARLY ONLINE RELEASE

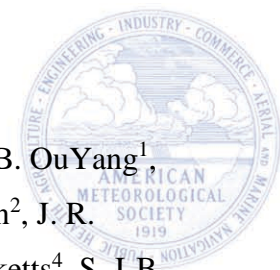
This is a preliminary PDF of the author-produced manuscript that has been peer-reviewed and accepted for publication. Since it is being posted so soon after acceptance, it has not yet been copyedited, formatted, or processed by AMS Publications. This preliminary version of the manuscript may be downloaded, distributed, and cited, but please be aware that there will be visual differences and possibly some content differences between this version and the final published version.

The DOI for this manuscript is doi: 10.1175/BAMS-D-14-00290.1

The final published version of this manuscript will replace the preliminary version at the above DOI once it is available.

If you would like to cite this EOR in a separate work, please use the following full citation:

Harris, N., L. Carpenter, J. Lee, G. Vaughan, M. Filus, R. Jones, B. OuYang, J. Pyle, A. Robinson, S. Andrews, A. Lewis, J. Minaeian, A. Vaughan, J. Dorsey, M. Gallagher, M. Le Breton, R. Newton, C. Percival, H. Ricketts, S. Bauguitte, G. Nott, A. Wellpott, M. Ashfold, J. Flemming, R. Butler, P. Palmer, P. Kaye, C. Stopford, C. Chemel, H. Boesch, N. Humpage, A. Vick, A. MacKenzie, R. Hyde, P. Angelov, E. Meneguz, and A. Manning, 2016: Co-ordinated Airborne Studies in the Tropics (CAST). *Bull. Amer. Meteor. Soc.* doi:10.1175/BAMS-D-14-00290.1, in press.



1 **Co-ordinated Airborne Studies in the Tropics (CAST)**

2 N. R. P. Harris^{1*}, L. J. Carpenter², J. D. Lee³, G. Vaughan⁴, M. T. Filus¹, R. L. Jones¹, B. OuYang¹,
3 J. A. Pyle^{1,5}, A. D. Robinson¹, S. J. Andrews², A. C. Lewis^{2,3}, J. Minaeian², A. Vaughan², J. R.
4 Dorsey^{4,6}, M. W. Gallagher⁶, M. Le Breton⁶, R. Newton⁶, C. J. Percival⁶, H. M. A. Ricketts⁴, S. J-B.
5 Baugitte⁷, G. J. Nott⁷, A. Wellpott⁷, M. J. Ashfold⁸, J. Flemming⁹, R. Butler¹⁰, P. I. Palmer¹⁰, P. H.
6 Kaye¹¹, C. Stopford¹¹, C. Chemel^{11,12}, H. Boesch^{13,14}, N. Humpage¹³, A. Vick¹⁵, A. R. MacKenzie¹⁶,
7 R. Hyde¹⁷, P. Angelov¹⁷, E. Meneguz¹⁸, A. J. Manning¹⁸.

8

- 9 1. Department of Chemistry, University of Cambridge, Cambridge, UK
10 2. Department of Chemistry, Wolfson Atmospheric Chemistry Laboratories, University of York,
11 York, UK
12 3. National Centre for Atmospheric Science (NCAS), York, UK
13 4. National Centre for Atmospheric Science (NCAS), Manchester, UK
14 5. National Centre for Atmospheric Science (NCAS), Cambridge, UK
15 6. School of Earth, Atmospheric and Environmental Science, University of Manchester,
16 Manchester, UK
17 7. Facility for Airborne Atmospheric Measurements, Cranfield, UK
18 8. School of Biosciences, University of Nottingham Malaysia Campus, Jalan Broga, 43500
19 Semenyih, Selangor, Malaysia
20 9. European Centre for Medium-Range Weather Forecasts, Reading, UK
21 10. School of GeoSciences, University of Edinburgh, Edinburgh, UK
22 11. Centre for Atmospheric & Instrumentation Research, University of Hertfordshire, Hatfield, UK
23 12. National Centre for Atmospheric Science (NCAS), University of Hertfordshire, Hatfield, UK
24 13. Earth Observation Science, Department of Physics and Astronomy, University of Leicester,
25 Leicester, UK
26 14. National Centre for Earth Observation, University of Leicester, UK
27 15. UK Astronomy Technology Centre, Edinburgh, UK
28 16. Birmingham Institute of Forest Research, University of Birmingham, Birmingham, UK
29 17. Data Science Group, Lancaster University, Lancaster, UK
30 18. Met Office, Exeter, UK

31 * now at Centre for Atmospheric Informatics and Emissions Technology, Cranfield University,
32 Cranfield, UK

33

34 Corresponding author:

35 Neil Harris, Centre for Atmospheric Informatics and Emissions Technology, Building 146,
36 Cranfield University, Cranfield, Bedfordshire, MK43 0AL, UK
37 E-mail: Neil.Harris@ozone-sec.ch.cam.ac.uk and Neil.Harris@cranfield.ac.uk

38

39 **Abstract**

40 The main field activities of the CAST (Co-ordinated Airborne Studies in the Tropics) campaign
41 took place in the West Pacific in January/February 2014. The field campaign was based in Guam
42 (13.5°N, 144.8°E) using the UK FAAM BAe-146 atmospheric research aircraft and was
43 coordinated with the ATTREX project with the unmanned Global Hawk and the CONTRAST
44 campaign with the Gulfstream V aircraft. Together, the three aircraft were able to make detailed
45 measurements of atmospheric structure and composition from the ocean surface to 20 km. These
46 measurements are providing new information about the processes influencing halogen and ozone
47 levels in the tropical West Pacific as well as the importance of trace gas transport in convection for
48 the upper troposphere and stratosphere. The FAAM aircraft made a total of 25 flights between 1°S-
49 14°N and 130°-155°E. It was used to sample at altitudes below 8 km with much of the time spent in
50 the marine boundary layer. It measured a range of chemical species, and sampled extensively within
51 the region of main inflow into the strong West Pacific convection. The CAST team also made
52 ground-based measurements of a number of species (including daily ozonesondes) at the
53 Atmospheric Radiation Measurement program site on Manus Island, Papua New Guinea (2.1°S,
54 147.4°E). This article presents an overview of the CAST project focussing on the design and
55 operation of the West Pacific experiment. It additionally discusses some new developments in
56 CAST, including flights of new instruments on the Global Hawk in February/March 2015.

57

58 **Capsule:** The Co-ordinated Airborne Studies in the Tropics (CAST) project is studying the
59 chemical composition of the atmosphere in the Tropical Warm Pool region to improve
60 understanding of trace gas transport in convection.

61

62 **Introduction**

63 The Tropical Tropopause Layer (TTL) is the region of the tropical atmosphere between the main
64 convective outflow at ~12-13 km and the base of the stratosphere at 17-18 km and is a very
65 important region for composition-aerosol-climate interactions (Randel and Jensen, 2013). Its overall
66 structure is intermediate between the troposphere and stratosphere, with a lapse rate smaller than the
67 saturated adiabatic up to the cold point (Fueglistaler et al., 2009). This is caused by the combined
68 effect of slow radiative processes and the infrequent penetration of convective turrets to high

69 altitude. There is a marked longitudinal asymmetry in TTL temperatures, with a minimum in the
70 region 130-180°E at all times of the year. This minimum corresponds to the warm waters of the
71 Tropical Warm Pool (TWP) beneath, and there is an associated maximum in convection (Gettelman
72 et al., 2002). The TTL is the predominant route for troposphere to stratosphere transport, so that
73 conditions in the TTL set the entry concentrations at the base of the stratosphere for, e.g.,
74 stratospheric water vapour and very short-lived halogen species. Knowledge of the input into the
75 TTL is a pre-requisite for correct modelling of TTL (and hence stratospheric) composition and yet
76 many aspects are poorly constrained (Levine et al., 2007; Heyes et al., 2009). The coupling between
77 the various processes are important. For example, improving the treatment of TTL water vapour
78 and cirrus in global climate models requires a better understanding of convective transport and
79 radiative transfer in the TTL, as well as improved model descriptions of the key processes.

80 We are still unclear about the entry and exit routes for the TTL, including how much material is
81 transported quasi-horizontally into the extratropical lowermost stratosphere (Levine et al., 2008).
82 What is the average residence time in the TTL? What is the nature, and importance for composition,
83 of longitudinal variability within the TTL? How much of the very short-lived halogen species can
84 pass through the TTL and so affect stratospheric ozone concentrations? Large discrepancies exist
85 between models and measurements even for long-lived tracers. Some of these are due to transport –
86 sharp horizontal gradients are observed in atmospheric tracers at boundaries between mid-latitude,
87 subtropical and tropical airmasses which are not well represented by models (Wofsy et al., 2011) –
88 and some to limited information on emissions, e.g. N₂O and CH₄ in this region (Ishijima et al.,
89 2010). These issues are more important for very short-lived substances (VSLS - lifetimes < 6
90 months), including halogen-containing VSLS with their poorly understood sources, atmospheric
91 transformations and geographic distribution (Carpenter, Reimann et al., 2014). Other effects such as
92 the degree to which the locations of the emissions coincide with strong convection can also have a
93 strong influence on the overall flux (Russo et al., 2015).

94 To address these issues, the Facility for Airborne Atmospheric Measurements (FAAM) BAe-146
95 atmospheric research aircraft was deployed in Guam in January and February 2014 as part of Co-
96 ordinated Airborne Studies in the Tropics (CAST), a large multi-institutional project funded by
97 the UK Natural Environment Research Council (NERC) and Science and Technology Facilities
98 Council (STFC). In Guam, it flew alongside the NASA Global Hawk, a high altitude autonomous
99 aircraft used in the NASA Airborne Tropical Tropopause Experiment (ATTREX) project, and the
100 NSF/NCAR Gulfstream V (GV) in the NSF Convective Transport of Active Species in the Tropics
101 (CONTRAST) project, as described in the companion papers, Jensen et al. (2016) and Pan et al.

102 (2016). The measurements from all three campaigns are being jointly used to diagnose how air is
103 carried high into the atmosphere.

104 The value inherent in having the three aircraft flying together was to be able to measure from the
105 surface up into the stratosphere (see Figure 1 in Pan et al., 2016). The instrument payloads on the
106 three aircraft made many common measurements which together have combined to provide a
107 comprehensive data set for interpretative studies. However within this larger picture, each aircraft
108 had its own scientific aims and objectives which were appropriate to the specific aircraft
109 capabilities. The Global Hawk made measurements in upper tropical TTL (14-20 km), including in
110 the outflow of convection. The GV aircraft principally sampled at the same altitudes as the main
111 convective outflow (9-15 km), and additionally made measurements on profiles down into the
112 boundary layer. In the case of the FAAM aircraft, the aims were to (i) investigate halocarbon
113 production in the marine boundary layer, and (ii) characterise the composition of air in the main
114 convective inflow. Knowledge of the distributions of trace gases in the boundary layer and lower
115 troposphere is needed to estimate the flux of these gases into the TTL. The role of the FAAM
116 research aircraft was to fly over the tropical West Pacific and to measure the composition in the low
117 troposphere (0-8 km). These measurements characterise the air masses in the region of the main
118 convective inflow and so are valuable in interpreting the higher altitude measurements of the Global
119 Hawk and the GV made in the same period. They can also be used to improve understanding of
120 marine halocarbon production and to investigate the influence of polluted outflow from Asia.
121 Additional measurements were made on Manus, Papua New Guinea.

122 The majority of this paper describes the CAST measurements in January/February 2014, and the
123 flight planning tools used for the FAAM aircraft and for linking its measurements with those made
124 by the other aircraft. Some early results are also discussed. The second CAST goal is to develop the
125 UK capability to use autonomous aircraft for atmospheric research. Here, in addition to learning
126 about deploying the Global Hawk and using the data collected, CAST scientists have produced two
127 new instruments for use on the Global Hawk which flew over the East Pacific in February/March
128 2015. These are described in the final section.

129

130 **CAST measurements**

131 Measurements were made on two main platforms in the West Pacific. The FAAM BAe-146
132 research aircraft was based at the A.B. Won Pat International Airport, Guam (13.5°N, 144.8°E).
133 The FAAM aircraft was co-located with the NCAR Gulfstream while the NASA Global Hawk was
134 based at Andersen Air Force Base approximately 30km to the north east. A suite of ground-based
135 instrument systems was based at the Atmospheric Radiation Measurement (ARM) facility at

136 Manus, Papua New Guinea (2.1°S, 147.4°E), in order to characterise the tropospheric composition
137 beyond the range of the FAAM aircraft.

138

139 *Flight planning*

140 The goal of the CAST FAAM flights was to characterise the inflow to convection in the lower
141 troposphere in the West Pacific. In order to extend the range of the aircraft so that it could reach
142 into the upwelling area near the equator, overnight stops were planned at the islands of Palau
143 (Roman Tmetuchl International Airport, Babeldaob island, Republic of Palau; 7.4°N 134.5°E) and
144 Chuuk (Chuuk International Airport, Weno Island, Federated States of Micronesia; 7.5°N,
145 151.8°E). When conditions allowed, transects were made at 100 feet (with occasional dips down to
146 50 feet) over the open ocean to give the opportunity to sample air influenced by fresh ocean
147 emissions. Stacked runs with horizontal legs at different altitudes were planned where possible to
148 provide information about the vertical profile of the short-lived species in the lower troposphere. A
149 large part of the flight planning for the FAAM research aircraft was to ensure a good coverage of
150 the lower troposphere within range from Guam.

151 Chemical forecast products were provided by the Monitoring Atmospheric Composition & Climate
152 (MACC) project in support of all three field campaigns. MACC assimilates comprehensive global
153 observations of chemical composition into the ECMWF meteorological forecasting system
154 (Flemming et al., 2015). The operational MACC system runs at 80 km horizontal resolution (T255)
155 with 60 vertical levels. During the campaign, forecast plots for the operation domain were provided
156 for a number of chemical species, including the FAAM measurements: O₃, CO, CH₄, black carbon,
157 NO, and NO₂. In addition, a number of hypothetical tracers were included to track air originating
158 from different locations, e.g. regional emissions from China and India. A coastal emission tracer
159 was used to track oceanic emissions of CHBr₃ and other short-lived halocarbons since these are
160 preferentially released in coastal regions (Carpenter et al., 2009; Ashfold et al., 2014).

161

162 *Linking measurements*

163 In order to have near-real-time information about the air reaching the TTL from the lower
164 troposphere, the trajectory-based approach of Ashfold et al (2012) was adapted to meet the needs of
165 a multi-aircraft campaign. In this, the Numerical Atmospheric-dispersion Modelling Environment
166 (NAME) was run as an adjunct to the Met Office operational forecasting model so that it could
167 access meteorological forecasts on a timescale quick enough to provide useful flight planning
168 information. The starting grid for the trajectories covered a large area of the West Pacific (Figure
169 7), with trajectories being released at altitudes between 8 and 18 km. Twelve day backward

170 trajectories were then calculated using a mixture of Met Office analyses and forecasts, so that
171 information was available about the possible influence of lower tropospheric air in the regions
172 which could be sampled by the Global Hawk and the GV. Each day, trajectories were produced for
173 1, 2, 3 and 5 days in the future. In each 2 km altitude layer, 5,000 particles were released in each 10°
174 $\times 10^\circ$ box. During the campaign, these calculations were made for a larger area at higher altitudes to
175 reflect the larger range of the Global Hawk. The horizontal resolution of the Met Office operational
176 model was 25 km in early 2014.

177 An example is shown in Figure 1 for three altitude ranges (12-14 km, 14-16 km, and 16-18 km).
178 Each point is the end-point of each parcel of air that had crossed below 1 km in the preceding 12
179 days. For graphical clarity, only a fraction of the trajectories are shown at each level. Thus strong,
180 predicted low level influence is indicated by a high percentage in each box (shown by the number),
181 and at a given level by the denser clouds. These maps were routinely checked against flight plans
182 for the Global Hawk and the GV to ensure that a wide range of low level influence was sampled. In
183 general, most flight plans met this criteria due to the proximity of the aircraft to the main convective
184 region.

185

186 ***FAAM BAe-146 aircraft***

187 The FAAM BAe-146 has a science payload of up to 4 tonnes devised according to the objectives of
188 a particular campaign. The chemical composition of the tropical atmosphere is the focus of CAST
189 and this dictated the scientific payload. The chemical species and physical parameters measured on
190 the FAAM aircraft, along with the instruments used, are summarised in Table 1. Trace gases with a
191 wide range of atmospheric lifetimes, sources and sinks were measured in order to provide
192 information about the origin and fate of the air masses encountered as well as about the atmospheric
193 timescales involved. In many cases these species were also measured by the Global Hawk and/or
194 the GV aircraft giving good synergy between the three datasets. Understanding the distribution and
195 chemistry of halogen species is a special focus for all three campaigns and this is reflected in the
196 FAAM payload.

197 Whole air samples (WAS) were collected as described in Andrews et al. (2013). Analysis of WAS
198 canisters was carried out in the aircraft hangar, usually within 72 hours of collection. Two litres of
199 sample air were pre-concentrated using a thermal desorption unit (Markes Unity2 CIA-T) and
200 analysed with gas chromatography, mass spectrometry (GC-MS, Agilent 7890 GC, 5977 Xtr MSD).
201 Halocarbons were quantified using a NOAA calibration gas standard. Dimethylsulfide was
202 quantified using a secondary standard prepared and referenced to a primary KRISS standard. The
203 full method is detailed in Andrews et al. (2013, 2016).

204 Measurements of a subset of halocarbons and other volatile organic compounds (VOCs) were made
205 in-flight using a new thermal desorption (TD) GC-MS system. 1 L of sample air, drawn from a
206 window blank inlet, pressurised to 2.5 atm and dried using a multi-core counter-current Nafion drier
207 was alternately pre-concentrated or analysed from two parallel adsorption traps (Tenax TA) of
208 a two channel TD system (Markes International, model TT 24/7). Analytes were refocussed at the
209 head of the column using liquid CO₂ prior to separation (10 m, 180 micron I.D., 1 micron film,
210 Restek RTX502.2 column; 40 to 150 °C at 40 °C min⁻¹) by GC (Agilent 6850) and detection by
211 electron impact MS single ion monitoring (Agilent 5975C), calibrated pre-flight against the WAS
212 gas standard (NOAA, SX-3581). Instrument temporal resolution, and associated sample integration
213 period, was 5 min.

214 The chemical ionisation mass spectrometer (CIMS) from the Georgia Institute of Technology was
215 configured similarly to previous deployments (Le Breton et al., 2012; 2013). The I⁻ ionization
216 scheme was used to detect inorganic halogens, carboxylic acids, HCN and other trace species. For
217 CAST, the CIMS made simultaneous measurements of BrO, BrCl, Br₂ and HOBr. The 1 Hz data
218 were averaged to 30 s for analysis. Pre-campaign and post-flight laboratory calibrations were used
219 relative to in-flight formic acid calibrations to quantify the sensitivities and limits of detection for
220 the inorganic halogens, similar to that used for dinitrogen pentoxide (Le Breton *et al.*, 2014). The
221 sensitivities ranged from 1 to 50 ion counts ppt⁻¹ s⁻¹ determined by in-flight and post-campaign
222 calibrations. The limits of detection for species varied from 0.36 ppt to 37 ppt for 30 s averaged
223 data. (All mixing ratios given in this paper are by volume.) An acid scrubber was used to quantify
224 background signal in the instrument and inlet line.

225 A broadband cavity-enhanced absorption spectrometer (BBCEAS) was adapted to measure IO in
226 the 410-482 nm wavelength region. No clear absorption feature was observable from spectra by eye
227 with up to 100 s averaging, pointing to very low mixing ratios (<~0.5 ppt) of IO over the sampled
228 area. When using averaged data, a small positive bias (~0.3 ppt) of IO was observed with respect to
229 the zero. These observations appear to support the existence of IO in the remote marine boundary
230 layer at sub-ppt levels, but the limited sensitivity precludes robust identification of spatial gradients.

231 NO was measured using chemiluminescence. NO₂ was quantified using a second channel, with NO₂
232 being converted to NO using a blue light LED converter centred at 395 nm. The NO₂ mixing ratio is
233 derived from the difference between total NO_x and NO mixing ratios. The instrument is calibrated
234 via addition of 5 sccm of known NO concentration to the ambient sample. The conversion
235 efficiency of the LED converter is measured in each calibration using gas phase titration of the NO
236 to NO₂ on addition of O₃. In flight calibrations were conducted above the boundary layer to ensure

237 stable low levels of NO_x with before and after flight calibrations made using an overflow at the inlet
238 of zero grade air. A more detailed description of a similar system can be found in Lee et al. (2009).

239 O₃ was measured by a UV absorption photometer (Thermo Fisher, model 49C), traceable to the UK
240 National Physical Laboratory primary ozone standard with an uncertainty of 2%, and a precision of
241 1 ppb for 4 s measurements.

242 CO was measured by a vacuum UV fluorescence analyser (Aero Laser GmbH, model AL5002,
243 Gerbig et al., 1999). The instrument was calibrated in-flight every ~45 minutes using a synthetic air
244 working standard (Air Liquide, ~500 ppb), traceable to the NOAA-Earth System Research
245 Laboratory (GMD-CCGG) surveillance standard and the World Meteorological Organisation CO
246 scale X2004. 1 Hz CO measurements have a 2% uncertainty and 3 ppb precision.

247 CO₂ and CH₄ were measured by a cavity-enhanced IR absorption spectrometer (Los Gatos Research
248 Inc. Fast Greenhouse Gas Analyser, model RMT-200). The instrument was customised for airborne
249 operation (O'Shea et al, 2013), so CO₂ and CH₄ dry mole fractions can be linearised in-flight using
250 natural air working standards, traceable to the World Meteorological Organisation CO₂ scale X2007
251 and CH₄ scale X2004. The performance of the system is estimated from the 1 σ standard deviation
252 of all in-flight 'target' calibration data. The 1 Hz measurement precisions are estimated at 0.7 ppm
253 and 2.5 ppb for CO₂ and CH₄. Through the addition of all known uncertainties we estimate a total
254 accuracy of ± 1.3 ppb for CH₄ and ± 0.2 ppm for CO₂.

255 The Passive Cavity Aerosol Spectrometer Probe 100-X (PCASP), upgraded with the SPP-200
256 electronics package from Droplet Measurement Technologies (DMT), measures aerosol particles
257 with nominal diameters 0.1 to 3 μm . Light from a 0.6328 μm laser is scattered by the particles and a
258 photodetector sums the forward (over solid angles subtended by 35°-120°) and backward (60°-
259 145°) scattered light. The probe is canister-mounted under the wing and was operated at 1 Hz. The
260 instrument was calibrated for particle size before and after the campaign. Uncertainties exist in both
261 the sizing and counting of particles and these are discussed, along with the calibration procedure, in
262 Rosenberg et al. [2012].

263 The DMT Cloud Droplet Probe (CDP; Lance et al., 2010) was flown on the same under-wing pylon
264 as the PCASP. The CDP is an open path instrument that measures the forward scattered light (over
265 solid angles nominally subtended by 1.7°-14°) from the 0.658 μm incident laser beam. Particles are
266 assigned to one of thirty size bins over the nominal size range 3-50 μm . Calibration with certified
267 diameter glass beads was carried out before each flight (Rosenberg et al., 2012). The sample rate of
268 the CDP was the same as for the PCASP, 1 Hz.

269

270 *Manus*

271 Observations started at the ARM Climate facility on Manus Island in October 1996 (Mather et al,
272 1998) and continued until August 2014. These observations provided the basis for many studies of
273 the climate in the West Pacific (e.g., Long et al., 2013 and references therein). In February 2014, a
274 suite of ground-based instruments was deployed as part of CAST to make measurements of ozone
275 (ground and profile), short-lived halocarbons, carbon dioxide, carbon monoxide and methane. The
276 instruments used are now described and are summarised in Table 2.

277 Ozone profiles were measured using ozonesondes. Air is pumped through a KI solution in a cathode
278 half-cell, with two electrons produced for each ozone molecule; the cell current is directly
279 proportional to the flow of ozone through the cell. Ozonesondes have a typical response time of ~ 1
280 minute at the tropopause level, with a precision of a few ppb. In the TTL the accuracy of the
281 measurement is dominated by the background current (Newton et al., 2016 and references therein).
282 Simultaneously, vertical profiles of temperature, humidity, wind and pressure were measured with
283 Vaisala RS92 radiosondes.

284 Ground-level ozone was measured by a Thermo-Electric Corporation TE49C which is a dual-
285 channel ultraviolet photometer measuring ozone through absorption of radiation at 254 nm. The
286 incoming air stream is split between two identical cells, with a scrubber removing ozone from one
287 of the streams. The TE49C provides a measurement every 10 s and has a 20 s response time.

288 Ground-level trace gas concentrations were measured by a Picarro Cavity Ring-Down Spectrometer
289 G2401 (CRDS) (Crosson, 2008). The sample air inlet was at ~8 m above ground level with a rain
290 cover and a 2 μm particulate filter. Water vapour in the instrument was kept below 1.5 ppm and was
291 controlled by passing the sample flow (~250 mL min⁻¹) through a chiller at ~5 °C and then through
292 a dessicant-based nafion drier. CO₂ and CH₄ concentrations were recorded every 5 s, with
293 precisions of ~1 ppb and ~200 ppb respectively. Calibrations were achieved using a target gas
294 (CH₄, 2024 ppb; CO₂, 390 ppm) measured every 2 days for 10 minutes with low / high calibration
295 runs on intermediate days (low/high: CH₄, 1919/2736 ppb; CO₂, 360/495 ppm). The calibration
296 gases are linked to the NOAA/WMO calibration scale.

297 Surface concentrations of short-lived halocarbons were measured using a μDirac instrument, a gas
298 chromatograph with electron capture detector (GC-ECD) based on that described in Gostlow et al
299 (2010) but with a 10 m separation column. The instrument sampled ambient air from the ~ 8 m
300 high mast, with a 10-20 ml min⁻¹ flow dried using a counter flow nafion drier. Calibration runs,
301 using a NOAA-ESRL air cylinder spiked with the target compounds, were conducted regularly
302 (every 3 samples). The calibration volumes ranged from 3 to 50 ml to allow correction for drifts in

303 instrument sensitivity and linearity. Measurement precision is species dependent, typically 2-10 %
304 (± 1 sd), with accuracy in the range 5-10 % (± 1 sd).

305

306 **Overview of measurements**

307 The FAAM BAe-146 made a total of 25 science flights with 90 flight hours during the CAST
308 deployment in the West Pacific (Figure 2). Brief summaries of the flights are given in Table 3. The
309 flight tracks are shown in Figure 2, with the altitude represented by the colour of the line. The large
310 majority of the flights were below 5 km altitude, with a significant fraction in the marine boundary
311 layer (below ~ 1 km), with good coverage between 130°E - 160°E and 2°S - 14°N .

312 The vertical distribution of the science flights can also be seen in Figure 3 which shows O_3 and CO
313 concentrations as a function of altitude and latitude. In general lower O_3 values are found in the
314 marine boundary layer and at lower latitudes, while high values are found at higher altitudes and at
315 higher latitudes. There is no obvious correlation with CO. However when the O_3 and CO data are
316 plotted against each other (Figure 4), a bimodal relationship emerges. Further, the lower ozone
317 values (10-40 ppb) occur when the relative humidity is high (Figure 4, top panel). This finding
318 reinforces that of Pan et al. (2015) who report this bimodality throughout the altitude range covered
319 by the NCAR GV, with a background mode of nearly constant (~ 20 ppb) values throughout the
320 troposphere and a secondary mode of higher ozone (~ 35 - 95 ppb) in layers with lower relative
321 humidity. The previously reported S-shaped mean profile (Folkins et al., 2002) results from
322 averaging the two modes.

323 The CAST measurements (Figure 4) show that high ozone and lower relative humidity often occurs
324 with higher NO concentrations and do not occur with low CO concentrations. Preliminary analysis
325 of the high NO measurements indicates that the air masses encountered had previously been in
326 regions close to anthropogenic activities and/or biomass burning. For example, the MACC forecasts
327 show transport of biomass burning and SE Asian tracers to the West Pacific. The possible role of
328 biomass burning has been thoroughly investigated by Anderson et al. (2016) using CAST and
329 CONTRAST measurements. The presence of HCN, CH_3CN and other tracers in the high ozone
330 levels is explained by biomass burning plumes which are convectively lofted into the free
331 troposphere undergoing dehydration during the convection. As this air descends, its relative
332 humidity drops and ozone is produced photochemically.

333 The CHBr_3 concentrations measured with the Whole Air Sampler and the on-board GC-MS are
334 shown in Figure 5. In general the values are low with even the higher values not far above the
335 background values seen in this region (Brinckmann et al., 2012). The lower amounts of CHBr_3 were
336 encountered out of the boundary layer (Figure 4b). The background in Figure 2 shows that the

337 Chlorophyll-a concentrations in the surface waters of the West Pacific were low in this period.
338 Higher Chl-a values are seen in the shallower waters approaching the islands of the Maritime
339 Continent. The lagoon inside Chuuk atoll is relatively shallow (<60 m) and is embedded in much
340 deeper ocean waters. It has a circumference of ~200 km and an area of ~3000 km². If halocarbons
341 are emitted preferentially in shallow waters (Carpenter et al., 2009), then it should be discernible as
342 an emission hotspot. The influence of short-lived halocarbon emissions from shallower waters was
343 investigated in the FAAM flights by circling Chuuk atoll at low altitudes. The inset of Figure 5a
344 shows the CHBr₃ observed on these flights as well as the instantaneous wind speed observed by the
345 FAAM aircraft. Higher concentrations of CHBr₃ (red) are found when air has previously passed
346 over the atoll, indicating that the atoll is a source of CHBr₃.

347 The NAME model driven by Met Office analysed fields has been used to interpret the CHBr₃ and
348 other brominated VSLS measurements made near the tropopause on the Global Hawk in the East
349 Pacific in 2013 and the West Pacific in 2014 (Navarro et al., 2015). The approach is similar to the
350 forecast information produced during the campaign (see above). They find that the majority of air
351 recently injected into the TTL had come from the West Pacific in both years with similar amounts,
352 ~6 (4-9) ppt, of combined organic and inorganic bromine derived from brominated VSLS.

353 CHBr₃ was also observed at the ARM facility in Manus (Figure 5). The median value in this period
354 was 0.81 ppt, about half that previously observed at a coastal site in Malaysian Borneo (Robinson et
355 al., 2014) and similar to the values observed on the FAAM aircraft (Figure 4). A strong diurnal
356 cycle is seen in early February in several trace gases measured at Manus with increased nocturnal
357 amounts providing evidence for local night-time sources of CO₂, CH₄, CHBr₃ and CH₃I. This
358 diurnal behaviour was seen from February 3rd to 12th when the winds were low and a stable
359 boundary layer was able to form. Before and after this period winds were higher and the night-time
360 build-up was much less.

361 Together, the CHBr₃ observations appear consistent with past work focussed on Southeast Asia.
362 Elevated levels are frequently observed close to coasts (e.g. Pyle et al., 2011) or above shallow
363 waters, but measurements collected a relatively small distance away (less than a typical global
364 model grid cell) rarely contain above background levels of CHBr₃. This suggests that coasts are not
365 a large source in a regional/global sense (as found by Ashfold et al., 2014), and for coastal CHBr₃
366 emissions to contribute significantly to the TTL and stratosphere would require co-location of
367 convection (Russo et al., 2015).

368 Ground-based ozone at Manus showed decreases at night in the quiescent period from a peak
369 daytime value of 10 ppb to sub 5 ppb levels which are consistent with oxidative uptake to the local
370 vegetation (Figure 6). This is the only time such low values of ozone were seen in CAST. In the

371 absence of local sources, C_2Cl_4 is a good tracer of large scale transport, and its concentrations in
372 this period were generally in the range 1-1.5 ppt which are typical of those seen in the clean West
373 Pacific (Ashfold et al., 2015). Manus was mainly influenced by flow from the north in this period.
374 A total of 39 ozonesondes were launched from Manus in February 2014, with 34 sondes providing
375 good ozone profiles (Figure 7(a); Newton et al., 2016). These measurements are hardest in the
376 tropics as the ozone concentrations are low, so that any error in estimating the background current is
377 important. Particular attention was therefore paid to measurements of the background current,
378 leading to recommendations for changes to the standard operation procedures used in the sonde
379 preparation. Support for this approach is provided by good agreement in a coordinated ozonesonde /
380 GV flight (see Figure 14 in Pan et al., 2016). The ozone measurements are shown in Figure 7
381 alongside the corresponding MACC 1 and 4 day forecasts. The forecasts predicted the main
382 characteristics of the observations such as increased ozone at about 400 hPa from 14-16 Feb and the
383 low concentrations near the TTL from 19-23 Feb. The minimum reproducible ozone concentration
384 measured in the TTL was 12 ppb, consistent with the minimum of 13 ppb measured by the GV
385 during CONTRAST (Pan et al., 2016).

386

387 **New technology developments**

388 As part of the collaboration with ATTREX, three new developments were included in CAST: two
389 instruments for use on the Global Hawk, the Aerosol-Ice-Interface Transition Spectrometer (AIITS)
390 and the GreenHouse gas Observations in the Stratosphere and Troposphere (GHOST); and a
391 software tool, Real-time Atmospheric Science Cluster AnaLysis (RASCAL), designed to assist
392 aircraft scientists by performing real-time data analysis during flights. The two new instruments
393 were flown for a total of 40 hours in one test flight and two science flights in February-March 2015
394 from the NASA Armstrong Flight Research Center, California. They were part of a payload which
395 also included Hawkeye, the NOAA H_2O and O_3 instruments, the Global Hawk Whole Air Sampler
396 (GWAS), and Microwave Temperature Profiler (MTP) (see Jensen et al, 2016 for more details).

397 The Aerosol-Ice-Interface Transition Spectrometer (AIITS) was designed to probe different cirrus
398 regimes in the TTL in order to understand fundamental nucleation and sublimation processes
399 influencing the stratospheric water budget and fluxes, as well as the potential impact of biomass
400 burning on cirrus ice crystal activation and growth. It is the next instrument in the Small Ice
401 Detector (SID) family (Hirst et al., 2001; Kaye et al., 2008). AIITS acquires 2-D forward scattering
402 patterns from particles in the size range from about one to a few hundred micrometres and can
403 measure the depolarisation in backward and forward scattering. The patterns allow quantification of
404 the phase, habit and fine surface features of large aerosol and small ice crystals in the size range 2-

405 100 μm (Cotton et al., 2010; Ulanowski et al., 2014). Unique results were obtained by AIITS during
406 cirrus penetrations at 16.5 km and at temperatures down to -80°C (Figure 8). These revealed a
407 transition to smooth quasi-spherical ice particle regimes in specific regions of TTL layers in
408 response to changing supersaturation regimes. The impact on the radiative scattering properties of
409 cirrus in these regimes is being investigated.

410 GHOST is a novel grating spectrometer designed for remote sensing of greenhouse gases from
411 aircraft (Humpage et al., 2014). It measures spectrally-resolved shortwave-infrared radiance across
412 four spectral bands from 1.27 μm to 2.3 μm , with a spectral resolution between 0.1 and 0.3 nm. An
413 optical gimbal underneath the aircraft is programmed to pass solar radiation reflected from the
414 ocean surface through a fibre optic bundle into the spectrometer with a single grating and detector
415 for all 4 bands. The bands are chosen to include absorption bands for CO_2 and CH_4 as well as CO ,
416 H_2O and O_2 . O_2 is used to infer information on the scattering contributions towards the measured
417 light. The third Global Hawk flight of the CAST/ATTREX campaign targeted the overpasses of
418 two greenhouse gas observing satellites during clear sky conditions over the Eastern Pacific (Figure
419 9); the NASA Orbiting Carbon Observatory (OCO-2) and the JAXA Greenhouse gas Observing
420 SATellite (GOSAT). This Global Hawk flight therefore provides a very useful validation dataset for
421 these satellites, since they both make greenhouse gas measurements using a similar spectral range to
422 GHOST.

423 As real-time data becomes increasingly available, mission scientists are faced with a potentially
424 overwhelming data torrent from which they are required to find the information on which to base
425 decisions. At present, mission scientists often focus on a subset of the data stream, limiting the
426 depth of the analysis which can be carried out. As part of CAST, a new software framework,
427 RASCAL, has been developed based on recent developments in arbitrarily-shaped cluster detection
428 algorithms (Hyde and Angelov, 2015). It interfaces intuitively with mission scientist expert
429 knowledge and provides real-time on-the-fly cluster and anomaly detection (i.e. for real-time
430 diagnosis of structures such as those diagnosed in Figure 4, for example, but tested simultaneously
431 across many chemical 'dimensions'). The data stream can be separated in real-time, without a priori
432 assumptions about parameter relationships, to reveal different data groups and hence isolate specific
433 regions of interest that can be revisited virtually post-flight. In combination with the expert
434 knowledge of the mission scientists, support tools like RASCAL have the potential to be used on
435 many research aircraft, potentially adding significant value to the results achieved in field
436 measurement campaigns.

437

438 **Summary**

439 Based in Guam as part of a joint deployment with the NASA ATTREX Global Hawk and the NSF
440 CONTRAST GV, the FAAM research aircraft deployment in CAST has provided an excellent
441 characterisation of the lower tropospheric atmospheric composition in the Tropical Warm Pool
442 region. The majority of the FAAM aircraft flights were below 5 km altitude, and a significant
443 fraction was in the marine boundary layer with good coverage in 130°E-160°E and 2°S-14°N. A
444 suite of organic and inorganic halogen compounds was measured, with the bromine-containing
445 species particularly well covered.

446 Ground-based measurements were made at the ARM facility on Manus Island, Papua New Guinea
447 during February 2014. These measurements characterise the tropospheric composition just south of
448 the equator in a region inaccessible to the FAAM aircraft in this deployment. The Manus
449 ozonesonde measurements are a valuable resource, providing a good picture of the vertical
450 distribution of ozone in the Tropical Warm Pool region during February with a minimum ozone
451 concentration in the TTL of 12 ppb.

452 These measurements are being interpreted by CAST scientists in conjunction with measurements
453 from ATTREX and CONTRAST using a range of modelling and data analysis approaches. The
454 CAST data are stored at the British Atmospheric Data Centre (<http://badc.nerc.ac.uk/>), and
455 interested parties are encouraged to use them for their own studies. All users are strongly
456 encouraged to involve the responsible instrument scientists in these studies in order to have insight
457 into the strengths and weaknesses of these data.

458 Never before has the atmosphere over the West Pacific been observed in such detail, particularly
459 the chemical composition, with three aircraft covering all altitudes from 0 to 20 km. New insights
460 are starting to emerge with much improved understanding of the tropical ozone distribution (Pan et
461 al., 2015; Anderson et al., 2016; Newton et al., 2016). These will be underpinned by advances in the
462 understanding of halogen distribution (Navarro et al., 2015) and chemistry building on the new
463 tropospheric halogen measurements (Le Breton et al., 2016) and modelling (Sherwen et al., 2016).
464 Such research will lead to a much greater quantitative understanding of the role of (a) VLSL
465 reaching the stratosphere and (b) how halogen chemistry affects tropospheric ozone over the
466 tropical oceans. Similar advances can be expected with respect to transport and dynamics, the role
467 of cirrus cloud in climate and dehydration of the stratosphere. The benefits of this unique,
468 coordinated campaign are just starting to become clear.

469

470 **Acknowledgements**

471 CAST is funded by NERC and STFC, with grant NE/ I030054/1 (lead award), NE/J006262/1,
472 NE/J006238/1, NE/J006181/1, NE/J006211/1, NE/J006061/1, NE/J006157/1, NE/J006203/1,

473 NE/J00619X/1, and NE/J006173/1. N. R. P. Harris was supported by a NERC Advanced Research
474 Fellowship (NE/G014655/1). P. I. Palmer acknowledges his Royal Society Wolfson Research Merit
475 Award. The BAe-146-301 Atmospheric Research Aircraft is flown by Directflight Ltd and managed
476 by the Facility for Airborne Atmospheric Measurements, which is a joint entity of the Natural
477 Environment Research Council and the Met Office. The authors thank the staff at FAAM,
478 Directflight and Avalon Aero who worked so hard toward the success of the aircraft deployment in
479 Guam, especially for their untiring efforts when spending an unforeseen 9 days in Chuuk. We thank
480 the local staff at Chuuk and Palau, as well as the authorities in the Federated States of Micronesia
481 for their help in facilitating our research flights. Special thanks go to the personnel associated with
482 the ARM facility at Manus, Papua New Guinea without whose help the ground-based
483 measurements would not have been possible. Thanks to the British Atmospheric Data Centre
484 (BADC) for hosting our data and the NCAS Atmospheric Measurement Facility for providing the
485 radiosonde and ground-based ozone equipment. Chlorophyll-a data used in Figure 1 were extracted
486 using the Giovanni online data system, maintained by the NASA GES DISC. We acknowledge the
487 MODIS mission scientists and associated NASA personnel for the production of this data set.
488 Finally we thank many individuals associated with the ATTREX and CONTRAST campaigns for
489 their help in the logistical planning, and we would like to single out Jim Bresch for his excellent and
490 freely provided meteorological advice.

491

492 **References**

- 493 Acker, J. G., and G. Leptoukh, 2007: Online Analysis Enhances Use of NASA Earth Science Data.
494 *Eos, Trans.*, **88**, 2, 14-17.
- 495 Allen, G., and Coauthors, 2011: South East Pacific atmospheric composition and variability
496 sampled along 20° S during VOCALS-Rex. *Atmos. Chem. Phys.*, **11**, 5237-5262,
497 doi:10.5194/acp-11-5237-2011.
- 498 Anderson, D. C., and Coauthors, 2016: A Pervasive Role for Biomass Burning in Tropical High
499 Ozone/Low Water Structures, *Nature Communications*, **7**:10267, doi: 10.1038/ncomms10267.
- 500 Andrews, S. J., C. E. Jones, and L. J. Carpenter, 2013: Aircraft measurements of very short-lived
501 halocarbons over the tropical Atlantic Ocean. *Geophys. Res. Lett.*, **40**, 1005–1010,
502 doi:10.1002/grl.50141.
- 503 Andrews, S.A. and Coauthors, 2016: A comparison of very short-lived halocarbon (VSLS) aircraft
504 measurements in the West Tropical Pacific from CAST, ATTREX and CONTRAST. *In*
505 *preparation*.

506 Ashfold, M. J., N. R. P. Harris, E. L. Atlas, A. J. Manning and J. A. Pyle, 2012: Transport of short-
507 lived species into the Tropical Tropopause Layer. *Atmos. Chem. Phys.*, **12**, 6309-6322,
508 doi:10.5194/acp-12-6309-2012.

509 Ashfold, M. J., N. R. P. Harris, A. J. Manning, A. D. Robinson, N. J. Warwick, and J. A. Pyle,
510 2014: Estimates of tropical bromoform emissions using an inversion method. *Atmos. Chem.*
511 *Phys.*, **14**, 979–994, doi:10.5194/acp-14-979-2014.

512 Ashfold, M. J., and Coauthors, 2015: Rapid transport of East Asian pollution to the deep tropics.
513 *Atmos. Chem. Phys.*, **15**, 3565-3573, doi:10.5194/acp-15-3565-2015.

514 Brinckmann, S., A. Engel, H. Bönisch, B. Quack, and E. Atlas, 2012: Short-lived brominated
515 hydrocarbons – observations in the source regions and the tropical tropopause layer. *Atmos.*
516 *Chem. Phys.*, **12**, 1213-1228, doi:10.5194/acp-12-1213-2012.

517 Carpenter, L. J., C. E. Jones, R. M. Dunk, K. E. Hornsby, and J. Woeltjen, 2009: Air-sea fluxes of
518 biogenic bromine from the tropical and North Atlantic Ocean. *Atmos. Chem. Phys.*, **9**, 1805–
519 1816, doi:10.5194/acp-9-1805-2009.

520 Carpenter, L. J., S. Reimann, (Lead Authors), J. B. Burkholder, C. Clerbaux, B. D. Hall, R.
521 Hossaini, J. C. Laube, and S. A. Yvon-Lewis, 2014: Ozone-Depleting Substances (ODSs) and
522 Other Gases of Interest to the Montreal Protocol. Chapter 1 in Scientific Assessment of Ozone
523 Depletion: 2014, Update on Global Ozone Research and Monitoring Project – Report No. 55,
524 World Meteorological Organization, Geneva, Switzerland.

525 Cotton, R., Osborne, S., Ulanowski, Z., Hirst, E., Kaye, P. H., and Greenaway, R., 2010: The ability
526 of the Small Ice Detector, SID2 to characterise cloud particle and aerosol morphologies obtained
527 during flights of the FAAM BAe-146 research aircraft. *J. Atmos. Ocean. Tech.*, **27**, 290–303.

528 Crosson, E. R., 2008: A cavity ring-down analyzer for measuring atmospheric levels of methane,
529 carbon dioxide, and water vapor. *Appl. Phys. B*, **92**, 403–408, doi:10.1007/s00340-008-3135-y.

530 Flemming, J., and Coauthors, 2015: Tropospheric chemistry in the Integrated Forecasting System of
531 ECMWF. *Geosci. Model Dev.*, **8**, 975-1003, doi:10.5194/gmd-8-975-2015.

532 Folkins, I., C. Braun, A. M. Thompson, and J. Witte, 2002:, Tropical ozone as an indicator of deep
533 convection. *J. Geophys. Res.*, **107**, 4184, doi:10.1029/2001JD001178.

534 Fueglistaler, S., A. E. Dessler, T. J. Dunkerton, I. Folkins, Q. Fu, and P. W. Mote, 2009: Tropical
535 tropopause layer. *Rev. Geophys.*, **47**, RG1004, doi:10.1029/2008RG000267.

536 Gerbig, C., S. Schmitgen, D. Kley, A. Volz-Thomas, K. Dewey, and D. Haaks, 1999: An improved
537 fast-response VUV resonance fluorescence CO instrument. *J. Geophys. Res.*, **104**, 1699–1704.

538 Gettelman, A., M. L. Salby, and F. Sassi, 2002: Distribution and influence of convection in the
539 tropical tropopause region. *J. Geophys. Res.*, **107**, doi:10.1029/2001JD001048.

540 Gostlow B., A. D. Robinson, N. R. P. Harris, L. O'Brien, D. E. Oram, G. P. Mills, H. M. Newton,
541 S. E. Yong and J. A. Pyle, 2010: Micro-DIRAC: An Autonomous Instrument for Halocarbon
542 Measurements. *Atmos. Meas. Tech.*, **3**, 507-521, doi:10.5194/amt-3-507-2010.

543 Heyes, W. J., G. Vaughan, G. Allen, A. Volz-Thomas, H.-W. Pätz, and R. Busen, 2009:
544 Composition of the TTL over Darwin: local mixing or long-range transport? *Atmos. Chem.*
545 *Phys.*, **9**, 7725-7736, doi:10.5194/acp-9-7725-2009.

546 Hirst, E., P. H. Kaye, R. S. Greenaway, P. Field, and D. W. Johnson, 2001: Discrimination of
547 micrometre-sized ice and super-cooled droplets in mixed-phase cloud. *Atmos. Environ.*, **35**, 33–
548 47, doi:10.1016/S1352-2310(00)00377-0.

549 Hopkins, J. R., K. A. Read, and A. C. Lewis, 2003: A Two Column Method For Long-term
550 Monitoring Of Non-Methane Hydrocarbons (NMHCs) and Oxygenated Volatile Organic
551 Compounds. *J. Environ. Mon.*, **5**, 8-13.

552 Humpage, N., and Coauthors, 2014: GreenHouse Observations of the Stratosphere and Troposphere
553 (GHOST): a novel shortwave infrared spectrometer developed for the Global Hawk unmanned
554 aerial vehicle. *Proc. SPIE 9242, Remote Sensing of Clouds and the Atmosphere XIX; and Optics*
555 *in Atmospheric Propagation and Adaptive Systems XVII*, 92420P,
556 <http://dx.doi.org/10.1117/12.2067330>.

557 Hyde, R., and P. Angelov, 2015: A new online clustering approach for data in arbitrary shaped
558 clusters. 2015 IEEE 2nd International Conference on Cybernetics (CYBCONF), IEEE, 228-233,
559 doi:10.1109/CYBConf.2015.7175937.

560 Ishijima, K and Coauthors, 2010: Stratospheric influence on the seasonal cycle of nitrous oxide in
561 the troposphere as deduced from aircraft observations and model simulations. *J. Geophys. Res.*,
562 **115**, D20308, doi:10.1029/2009JD013322.

563 Jensen, E. J., and Coauthors, 2016: The NASA Airborne Tropical TRopopause EXperiment
564 (ATTREX): High-Altitude Aircraft Measurements in the Tropical Western Pacific. *Bull. Amer.*
565 *Meteor. Soc.*, submitted.

566 Kennedy, O. J., and Coauthors, 2011: An aircraft based three channel broadband cavity enhanced
567 absorption spectrometer for simultaneous measurements of NO₃, N₂O₅ and NO₂. *Atmos. Meas.*
568 *Tech.*, **4**, 1759-1776, doi:10.5194/amt-4-1759-2011.

569 Kaye, P.H., E. Hirst, R. S. Greenaway, Z. Ulanowski, E. Hesse, P. J. DeMott, C. Saunders, and P.
570 Connolly, 2008: Classifying atmospheric ice crystals by spatial light scattering. *Opt. Lett.*, **33**,
571 1545, doi:10.1364/OL.33.001545.

572 Lance, S., Brock, C. A., Rogers, D., and Gordon, J. A., 2010: Water droplet calibration of the Cloud
573 Droplet Probe (CDP) and in-flight performance in liquid, ice and mixed-phase clouds during
574 ARCPAC. *Atmos. Meas. Tech.*, **3**, 1683-1706, doi:10.5194/amt-3-1683-2010.

575 Le Breton, M., and Coauthors, 2012: Airborne observations of formic acid using a chemical
576 ionization mass spectrometer, *Atmos. Meas. Tech.*, **5**, 3029-3039, doi:10.5194/amt-5-3029-2012.

577 Le Breton, M., and Coauthors, 2013: Airborne hydrogen cyanide measurements using a chemical
578 ionisation mass spectrometer for the plume identification of biomass burning forest fires, *Atmos.*
579 *Chem. Phys.*, **13**, 9217-9232, doi:10.5194/acp-13-9217-2013.

580 Le Breton, M., and Coauthors, 2016: Active inorganic bromine chemistry in the tropical
581 troposphere, *J. Geophys. Res.*, *under review*.

582 Lee, J. D., S. J. Moller, K. A. Read, A. C. Lewis, L. Mendes, and L. J. Carpenter, 2009: Year-round
583 measurements of nitrogen oxides and ozone in the tropical North Atlantic marine boundary
584 layer. *J. Geophys. Res.*, **114**, D21302, DOI:10.1029/2009JD011878.

585 Lenschow, D. H., 1986: Probing the atmospheric boundary layer. Chap. in *Aircraft measurements*
586 *in the boundary layer*, 39–55, Amer. Meteor. Soc..

587 Levine, J. G., P. Braesicke, N. R. P. Harris, N. H. Savage, and J. A. Pyle, 2007: Pathways and
588 timescales for troposphere-to-stratosphere transport via the tropical tropopause layer and their
589 relevance for very short lived substances. *J. Geophys. Res.*, **112**, D04308,
590 doi:10.1029/2005JD006940.

591 Levine, J. G., P. Braesicke, N. R. P. Harris, and J. A. Pyle, 2008: Seasonal and inter-annual
592 variations in troposphere-to-stratosphere transport from the tropical tropopause layer. *Atmos.*
593 *Chem. Phys.*, **8**, 3689-3703, doi:10.5194/acp-8-3689-2008.

594 Liu, D., and Coauthors, 2015: The importance of Asia as a source of black carbon to the European
595 Arctic during springtime 2013. *Atmos. Chem. Phys.*, **15**, 11537-11555, doi:10.5194/acp-15-
596 11537-2015.

597 Long, C. N., and Coauthors, 2013: ARM Research In The Equatorial Western Pacific: A Decade
598 And Counting. *Bull. Amer. Meteor. Soc.*, **94**, 695–708. doi:10.1175/BAMS-D-11-00137.1.

599 Mather, J. H., T. P. Ackerman, W. E. Clements, F. J. Barnes, M. D. Ivey, L. D. Hatfield, and R. M.
600 Reynolds, 1998: An Atmospheric Radiation and Cloud Station in the Tropical Western Pacific.
601 *Bull. Amer. Meteor. Soc.*, **79**, 627–642. doi:10.1175/1520-0477.

602 Navarro, M. A., and Coauthors, 2015: Airborne measurements of organic bromine compounds in
603 the Pacific tropical tropopause layer. *Proc. Nat. Acad. Sci.*, **112**, 45, 13789-13793,
604 doi/10.1073/pnas.1511463112.

605 Newton, R., G. Vaughan, H. M. A. Ricketts, L. L. Pan, A. J. Weinheimer, and C. Chemel, 2015:
606 Ozonesonde profiles from the West Pacific Warm Pool: measurements and validation, *Atmos.*
607 *Chem. Phys.*, **16**, 619-634, doi:10.5194/acp-16-619-2016.

608 O'Shea, S. J., S. J.-B. Bauguitte, M. W. Gallagher, D. Lowry, and C. J. Percival, 2013:
609 Development of a cavity-enhanced absorption spectrometer for airborne measurements of CH₄
610 and CO₂. *Atmos. Meas. Tech.*, **6**, 1095-1109, doi:10.5194/amt-6-1095-2013.

611 Pan, L. L., and Co-authors, 2015: Bimodal distribution of free tropospheric ozone over the tropical
612 western Pacific revealed by airborne observations. *Geophys. Res. Lett.*, **42**,
613 doi:10.1002/2015GL065562.

614 Pan, L. L., and Co-authors, 2016: The Convective Transport of Active Species in the Tropics
615 (CONTRAST) Experiment. *Bull. Amer. Meteor. Soc.*, submitted.

616 Petersen, G. N., and I. A. Renfrew, 2009: Aircraft-based observations of air–sea fluxes over
617 Denmark Strait and the Irminger Sea during high wind speed conditions. *Q. J. R. Meteorol. Soc.*,
618 **135**, 2030–2045, 10.1002/qj.355.

619 Platnick, S., and Co-authors, 2015: MODIS Atmosphere L2 Cloud Product (06_L2). NASA
620 MODIS Adaptive Processing System, Goddard Space Flight Center, USA:
621 http://dx.doi.org/10.5067/MODIS/MYD06_L2.006.

622 Pyle, J. A., and Co-authors, 2011:, Bromoform in the tropical boundary layer of the Maritime
623 Continent during OP3, *Atmos. Chem. Phys.*, **11**, 529-542, [www.atmos-chem-](http://www.atmos-chem-phys.net/11/529/2011/)
624 [phys.net/11/529/2011/](http://www.atmos-chem-phys.net/11/529/2011/), 2011.

625 Randel, W., and E. Jensen, 2013: Physical processes in the tropical tropopause layer and their roles
626 in a changing climate. *Nature Geoscience*, **6**, 169-176, doi:10.1038/ngeo1733.

627 Robinson, A. D., and Co-authors, 2014: Long term halocarbon observations from a coastal and an
628 inland site in Sabah, Malaysian Borneo. *Atmos. Chem. Phys.*, **14**, 8369-8388, doi:10.5194/acp-
629 14-8369-2014.

630 Rosenberg, P. D., A. R. Dean, P. I. Williams, J. R. Dorsey, A. Minikin, M. A. Pickering, and A.
631 Petzold, 2012: Particle sizing calibration with refractive index correction for light scattering
632 optical particle counters and impacts upon PCASP and CDP data collected during the Fenec
633 campaign. *Atmos. Meas. Tech.*, **5**, 5, 1147-1163, 10.5194/amt-5-1147-2012.

634 Russo, M. R., M. J. Ashfold, N. R. P. Harris, and J. A. Pyle: On the emissions and transport of
635 bromoform: sensitivity to model resolution and emission location. *Atmos. Chem. Phys.*, **15**,
636 14031-14040, doi:10.5194/acp-15-14031-2015, 2015.

637 Sherwen, T., M. J. Evans, L. J. Carpenter, S. J. Andrews, R. T. Lidster, B. Dix, T. K. Koenig, R.
638 Volkamer, A. Saiz-Lopez, C. Prados-Roman, A. S. Mahajan, and C. Ordóñez: Iodine's impact on
639 tropospheric oxidants: a global model study in GEOS-Chem. *Atmos. Chem. Phys.*, in press,
640 2016.

641 Ström, J., R. Busen, M. Quante, B. Guillemet, P. R. A. Brown, and J. Heintzenberg, 1994: Pre-
642 EUCREX intercomparison of airborne humidity measuring instruments. *J. Atmos. Tech.*, **11**,
643 1392–1399, 1994.

644 Ulanowski, Z., P. H. Kaye, E. Hirst, R. S. Greenaway, R. J. Cotton, E. Hesse, and C. T. Collier,
645 2014: Incidence of rough and irregular atmospheric ice particles from Small Ice Detector 3
646 measurements. *Atmos. Chem. Phys.*, **14**, 1649-1662, doi:10.5194/acp-14-1649-2014.

647 Whalley, L. K., A. C. Lewis, J. B. McQuaid, R. M. Purvis, J. D. Lee, K. Stemmler, C. Zellweger,
648 and P. Ridgeon, 2004: Two high-speed, portable GC systems designed for the measurement of
649 nonmethane hydrocarbons and PAN: Results from the Jungfraujoch high altitude observatory. *J.*
650 *Env. Mon.*, **6**, 234-241.

651 Wilson, K. L., and J. W. Birks, 2006: Mechanism and elimination of a water vapor interference in
652 the measurement of ozone by UV absorbance. *Env. Sci. & Tech.*, **40**, 6361-6367, DOI:
653 10.1021/es052590c.

654 Wofsy, S. C., and Coauthors, 2011: HIAPER Pole-to-Pole Observations (HIPPO): fine-grained,
655 global-scale measurements of climatically important atmospheric gases and aerosols. *Phil.*
656 *Trans. R. Soc. A*, **369**, 2073–2086, doi: 10.1098/rsta.2010.0313.

657

658
659

Table 1: Instruments and measurements made on the BAe 146 (FAAM) aircraft during the CAST project. The table also indicates the synergy with other aircraft from the CONTRAST (Gulfstream-V (GV)) and ATTREX (Global Hawk (GH)) projects.

Species / parameter	Method / instrument details	Averaging time	Precision, accuracy	Synergy with other aircraft	Affiliation, reference
Position, winds, u, v, w	INS, GPS, 5-port turbulence probe	0.1 s	$0.01 \Delta P/P_s$	GV, GH	FAAM Peterson and Renfrew (2009)
Humidity (Dew point T)	Hygrometer, General Eastern 1011b	0.25 s	$\pm 0.5 - \pm 3$ K dependent on dew point and ambient conditions	GV, GH	FAAM Ström et al. (1994)
Temperature	Rosemount Aerospace Ltd. sensor 102 AL	.05 s	± 0.3 K	GV, GH	FAAM Lenschow (1986)
CO	VUV resonance / fluorescence, Aerolaser 5002	1 s	1 ppb, 3%	GV, GH	FAAM Gerbig et al. (1999)
O ₃	UV absorption, TEI 49C	4 s	1 ppb, $\pm 5\%$	GV, GH	FAAM Wilson and Birks (2006)
CO ₂ , CH ₄	Cavity enhanced absorption spectrometer, Los Gatos Research Inc	1 s	CH ₄ : 2.5 ppb; 1.3 ppm CO ₂ : 0.7 ppm; 0.2 ppm	GV, GH	FAAM / U. Manchester O'Shea et al. (2013)
NO, NO ₂	Chemiluminescence with photolytic conversion for NO ₂ , Air Quality Design Inc.	10 s	5 pptv for NO and 15 pptv for NO ₂ (at 10 s averaging)	GV	FAAM / U. York Lee et al. (2009)
Halocarbons (Whole air samples (WAS)): (DMS, CHBr ₃ , CH ₂ Br ₂ , CHBr ₂ Cl, CH ₃ I, CH ₂ BrCl, CHBrCl ₂ , CH ₂ ICl, CH ₂ I ₂ , CH ₂ Cl ₂ , CHCl ₃)	TD-GC-MS, Markes	30 s fill time for WAS	Species dependent, typically 0.1 – 1 pptv.	GV, GH	U. York Andrews et al. (2013; 2016)
NMHCs (Whole air samples (WAS)): (C ¹ -C ⁷ NMHCs (alkanes, alkenes, aromatics); small o-VOCs (acetone, methanol, acetaldehyde, ethanol); DMS	GC-FID (flame ionization detector), Perkin Elmer	30 s fill time for WAS	Species dependent, typically 5 pptv	GV, GH	U. York Hopkins et al. (2003)
Halocarbons, VOCs (<i>in situ</i>)	GC-MS (Gas Chromatography – Mass Spectrometry), Agilent	300 s	Species dependent, typically 1 – 5 pptv.	GV	U. York
BrO, Br ₂ , HOBr, BrCl, HCOOH (formic acid), HCN, ClNO ₂ , HNO ₃ , N ₂ O ₅ , CH ₃ COOH (acetic acid), CH ₃ CH ₂ COOH (propanoic acid), CH ₃ CH ₂ CH ₂ COOH (butanoic acid)	Chemical Ionisation Mass Spectrometer (CIMS)	30 s	Species dependent, typically 0.3 – 5 ppt	GV	U. Manchester Le Breton et al. (2012)
IO	Broadband Cavity Enhanced Absorption Spectrometer (BBCEAS)	<i>see text</i>	<i>see text</i>	GV (IO remote sensing)	U. Cambridge Kennedy et al. (2011)
PAN	Dual column GC-ECD	90 s	3%, 10%	GV	U. York Whalley et al. (2004)
Black carbon	Soot particle photometer (SP-2)	10 s		None	U. Manchester, Liu et al. (2015)

Aerosol	PCASP (Passive Cavity Aerosol Spectrometer Probe)	1s	See text	GV, GH	FAAM Rosenberg et al. (2012)
Cloud physics	CDP (Cloud Droplet Probe)	1s	See text	GV, GH	FAAM Rosenberg et al. (2012)

660
661
662
663

Table 2: Measurements made at the ARM site at Manus, Papua New Guinea during CAST

Species / parameter	Method / instrument details	Operation	Precision, accuracy	Affiliation, reference
O ₃ (profile)	Ozonesonde, ENSCI model Z from DMT	Daily	see Newton et al. (2016)	U. Manchester, NCAS Newton et al. (2016)
O ₃ (surface)	Thermo-49 analyser	Continuous (10 sec)	± 1 ppbv, precision-limited	NCAS, Atmospheric Measurement Facility
CO ₂ , CH ₄	Picarro G2401 CRDS analyser	Continuous (5 sec)	CO ₂ precision 0.05 %, accuracy 0.05 % (±1sd); CH ₄ precision 0.05 %, accuracy 0.1 % (±1sd);	U. Cambridge Crosson (2008)
Halocarbons: (CHBr ₃ , CHBr ₂ Cl, CH ₃ I, CH ₂ ICl, C ₂ Cl ₄)	Custom-built GC-ECD	Continuous (~50 minutes)	Species dependent, typically 0.1 – 1 pptv.	U. Cambridge Gostlow et al. (2010), Robinson et al. (2014)

664
665
666

Information about the meteorological measurements from Manus can be found at <http://www.arm.gov/sites/twp/C1/instruments>.

667 Table 3: Research flights made by the BAe 146 (FAAM) aircraft during the CAST project.

Flight no.	Date	Route	Flight description and observations
B823	18/1/14	Kota Kinabalu - Palau - Guam	Measurements on last part of leg from KK to Palau. Flight mainly at low levels (in boundary layer) on Palau to Guam leg. O ₃ and CO decreasing further North (O ₃ 30-12 ppb), higher (>35ppb) above boundary layer (BL).
B824	22/1/14	Guam – Guam	Heading SE from Guam, 4000 m then 2000 m, flight aborted early due to aircraft technical problem. GV followed around 30 minutes later. O ₃ 15 ppb near Guam, falling to 10 ppb at 7°S.
B825	24/1/14	Guam – Chuuk	Mixed altitudes (lowest 300 m), mainly within BL. O ₃ dropping from 15 ppb to 8 ppb towards Chuuk. CO ~105 ppb on whole flight. SE flow.
B826	25/1/14	Chuuk – Chuuk	Due South from Chuuk on 152°E to 2°N, back on 153°E. Start at 6000 m then step down to 300 m. O ₃ constant (~15 ppb) in boundary layer, 25 ppb above BL. Largely SE flow in BL, W-NW in free troposphere.
B827	26/1/14	Chuuk – Chuuk	Due South from Chuuk on 152°N to 1°N then return on same track. In BL to 1°N, 4000 m on return North. Well mixed boundary layer. 20 ppb O ₃ to 1°N. BrO and CH ₂ Cl ₂ observed. Largely SE flow in BL, W-NW in FT.
B828	26/1/14	Chuuk - Guam	Circled atoll at 100 m and 1500 m; then mixed altitude down to 300 m on way back to Guam. CO 100ppb round atoll in BL, O ₃ 15 ppb. O ₃ 10-13ppb as head North towards Guam.
B829	29/1/14	Guam - Palau	Mixed levels in BL down to 300 m. Low O ₃ (12 ppb) observed around island of Yap. Easterly flow.
B830	29/1/14	Palau – Palau	Flight East along 7°N; mixed altitude down to 300 m; 4 stacked runs above each other at easterly end. Profile of BrO observed on stacked runs - higher at surface. Same CO and O ₃ profile at all levels so well mixed BL. 45 ppb O ₃ and some NO _x (25 ppt) seen at 4000 m. Higher N ₂ O at higher altitudes. Largely SE flow.
B831	30/1/14	Palau – Palau	Flight SE to Indonesian airspace (4°30'N, 141°30'E) then due South to 3°N. Mainly in BL, down to 300 m at most Southern point where O ₃ was 25-30 ppb. Westerly flow so some Asian outflow observed (CO < 100 ppb).
B832	30/1/14	Palau – Guam	Low level runs in BL crossing day/night terminator. 30m in early part of flight before hitting low level convection. Above BL towards Guam. 15 ppb O ₃ during sunset - very constant as heading North. NW flow.
B833	1/2/14	Guam – Guam	1 st part of day/night chemistry flights. Stacked legs to E of Guam: 6000, 3000, 1500, 1000, and 300 m. NE flow. Followed GV for first half of flight (~30 minutes behind).
B834	1/2/14	Guam – Guam	2 nd part of day/night chemistry flights. Stacked legs to E of Guam: 6000, 3000, 1500, 1000, and 300 m. NE flow.
B835	4/2/14	Guam – Chuuk	Fast transit to Chuuk above BL. 25 ppb O ₃ , 85 ppb CO at 6000 m, then O ₃ lower as dropping down to Chuuk (~13 ppb).

B836	4/2/14	Chuuk – Chuuk	Head S along 152°E at 7000 m, some low flying in BL to southern most point (1°S) before intermediate height (2000 – 4000 m) back to Chuuk. 18 ppb O ₃ above BL to 1°N. Then profile down and less O ₃ in BL (13 ppb), CO 70 ppb. At 1°S O ₃ 9 ppb in NE flow.
B837	5/2/14	Chuuk – Chuuk	Low level flying in BL to southernmost point (~1°N) to complement B836), then climb back and return at ~5000 m. O ₃ decreasing in BL as head South. 20 ppb at 7°N, 11 ppb at 1°N. All in NE flow.
B838	6/2/14	Chuuk – Chuuk	Round Chuuk atoll at 3 altitudes in BL (150, 500, and 1000 m). CO higher to East of Islands (Easterly flow). Could be storms over the islands bringing elevated CO to the upwind side.
B839	12/2/14	Chuuk – Guam	SE of Guam at low level (500 m in BL), then above BL (5000 m) before descending down at lower levels in BL into Guam. O ₃ spikes in profiles up to 7500 m (Asian outflow). 75 ppb seen at 7000 m.
B840	13/2/14	Guam – Palau	Start in FT (~6500 m), then low nearer Palau (1500 m); head to 4°N, 137°E before heading NW; same region as GV and GH. O ₃ 30 ppb in FT, 12 ppb in BL, very stable. Easterly flow.
B841	14/2/14	Palau – Palau	Flight to SW of Palau with stacked legs in BL parallel to ATC boundary. O ₃ 15 ppb in BL. Easterly flow.
B842	14/2/14	Palau - Guam	Reverse flight to B840. Similar flow and O ₃ .
B843	16/2/14	Guam – Guam	S from Guam to 7°N then E towards Chuuk before heading back to Guam; low latitude parts at low altitudes (<1000 m in BL) under convective band. O ₃ 10-15 ppb in BL (E flow), elevated at higher levels (70-90 ppb), concurrent with elevated NO (30 ppt) (N flow).
B844	17/2/14	Guam – Guam	SSE from Guam to fly under convective band (to 4°N) with low level runs (< 1000 m in BL). GV and GH flying nearby. Layers of elevated O ₃ and NO _x at ~6000m (westerly flow).
B845	17/2/14	Guam – Guam	S from Guam to be West of convective band (to 6°N). Low level legs (< 1000 m in BL) at Southern end. Layers of elevated O ₃ and NO _x at ~6000 m (westerly flow).
B846	18/2/14	Guam - Palau	Start in FT (~6500 m), then low nearer Palau (1500 m); head to 4°N, 137°E before heading NW; same region as GV and GH. O ₃ 30 ppb in FT, 12 ppb in BL, very stable. Easterly flow.
B847	18/2/14	Palau – Kota Kinabalu	Steady ascent toward KK. Some Asian outflow observed on initial ascent (CO ~ 140 ppb). Westerly flow.

669 **Figure Caption List**

670 Figure 1. Examples of trajectory-based forecast products used for multi-aircraft flight planning.
671 These plots are for February 13 2014 when all three aircraft were in the same region
672 (see Figure 7 in Pan et al. (2016)). The three panels show the location of air parcels
673 which had been below 1 km altitude in the preceding 12 days at (a) 16-18 km; (b) 14-16
674 km; and (c) 12-14 km. The number in each box is the percentage of parcels in that box
675 from below 1 km in the preceding 12 days. During the campaign, they were available as
676 1, 3 and 5 day forecasts for flight planning, and the NAME model was driven by
677 analyses and forecasts from Met Office operational model run at 25 km horizontal
678 resolution.

679

680 Figure 2: Map of FAAM BAe-146 flight tracks during January and February 2014. The flights
681 tracks are coloured by altitude. The islands of Guam, Palau and Chuuk are marked. The
682 background shows Jan-Feb averaged Chlorophyll-a concentrations, measured by the
683 MODIS satellite (NASA Giovanni: Acker et al., 2007). The inset shows an enlarged
684 area around Chuuk Atoll.

685

686 Figure 3: Ozone and carbon monoxide mixing ratios measured in all CAST flights as a function
687 of latitude and altitude (left). The means and associated 2 standard deviations of ozone
688 and carbon monoxide are shown as a function of altitude (right). See text and Table 1
689 for instrumental details.

690

691 Figure 4: Plots of O₃ against CO coloured by (upper) NO and (lower) relative humidity (10 s
692 averaged data).

693

694 Figure 5: CHBr₃ mixing ratios (colours) sampled on the FAAM aircraft during CAST using the
695 whole air sampler (squares) and the on-board GC-MS (circles). Panel (a) contains all
696 measurements made at altitudes less than 1 km, and the enlarged inset (bottom left)
697 shows the values around the Chuuk Atoll. The lines associated with each measurement
698 in the inset indicate the instantaneous wind speed measured by the aircraft. Panel (b)
699 contains the measurements at altitudes greater than 1 km, and the inset shows the
700 vertical profile of all measurements.

701

702 Figure 6: Surface observations of wind, O₃, CO₂, CH₄, C₂Cl₄, CHBr₃ and CH₃I at the ARM
703 Facility on Manus Island, Papua New Guinea (2.07°S, 147.4°E) from February 1-24,

704 2014. The time shown in the x-axis is Universal Time. The shading indicates the local
705 time, with the darker bands representing night-time.

706

707 Figure 7: Daily observed ozone profile in Manus (left) and corresponding MACC forecast with a
708 lead time of 1 day (middle) and 4 days (right).

709

710 Figure 8: AITS scattering patterns recorded from ice particles in the UTLS, at altitudes of ~ 16
711 km and temperatures of ~ -80°C. The pictures are indicative of (left) a smooth quasi-
712 spherical ice particle, (middle) a columnar crystal, and (right) a pristine hexagonal plate.

713

714 Figure 9: Flight path of the NASA Global Hawk on 10th March 2015 (blue). OCO-2 (green) and
715 GOSAT (red) soundings are shown which coincide temporally with the flight leg
716 between 25°N, 127°W and 18°N, 125°W. MODIS cloud fraction data (Platnick et al.,
717 2015) coincident with the OCO-2 overpass at 2140 UTC is plotted in grayscale,
718 showing the largely cloud-free conditions encountered during this leg of the flight.

719

720

721

722

723

724

725

726

727

728

729

730

731

732

733

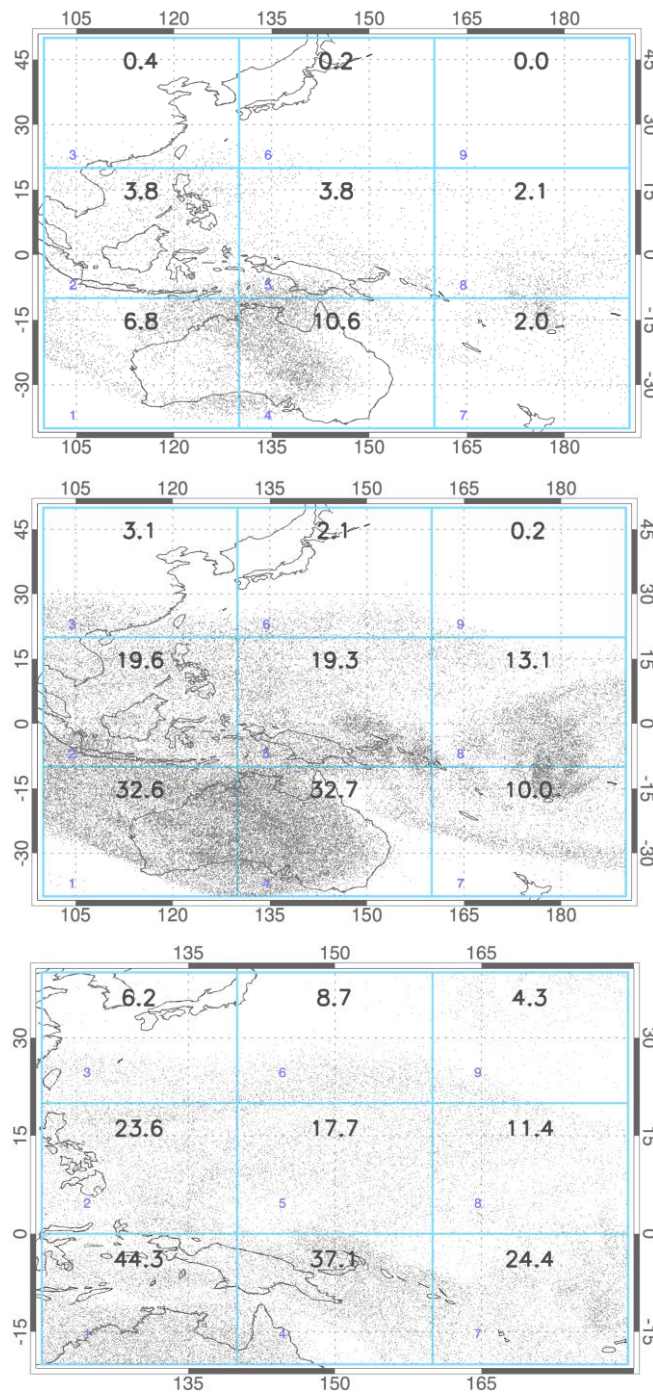
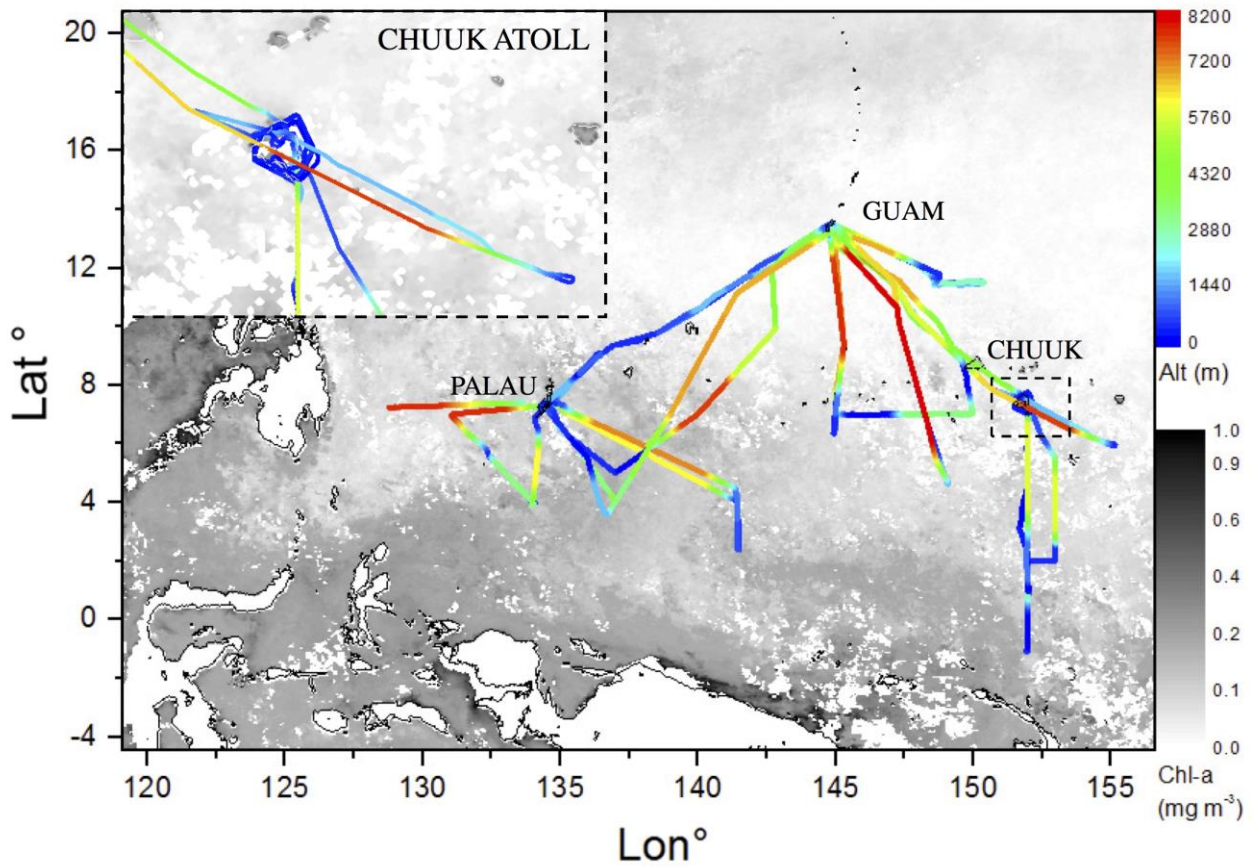


Figure 7. Examples of trajectory-based forecast products used for multi-aircraft flight planning. These plots are for February 13 2014 when all three aircraft were in the same region (see Figure 7 in Pan et al. (2016)). The three panels show the location of air parcels which had been below 1 km altitude in the preceding 12 days at (a) 16-18 km; (b) 14-16 km; and (c) 12-14 km. The number in each box is the percentage of parcels in that box from below 1 km in the preceding 12 days. During the campaign, they were available as 1, 3 and 5 day forecasts for flight planning, and the NAME model was driven by analyses and forecasts from Met Office operational model run at 25 km horizontal resolution. NB Only a fraction of the trajectories are shown in each plot, so the density of dots is not comparable at different altitudes.

734



735

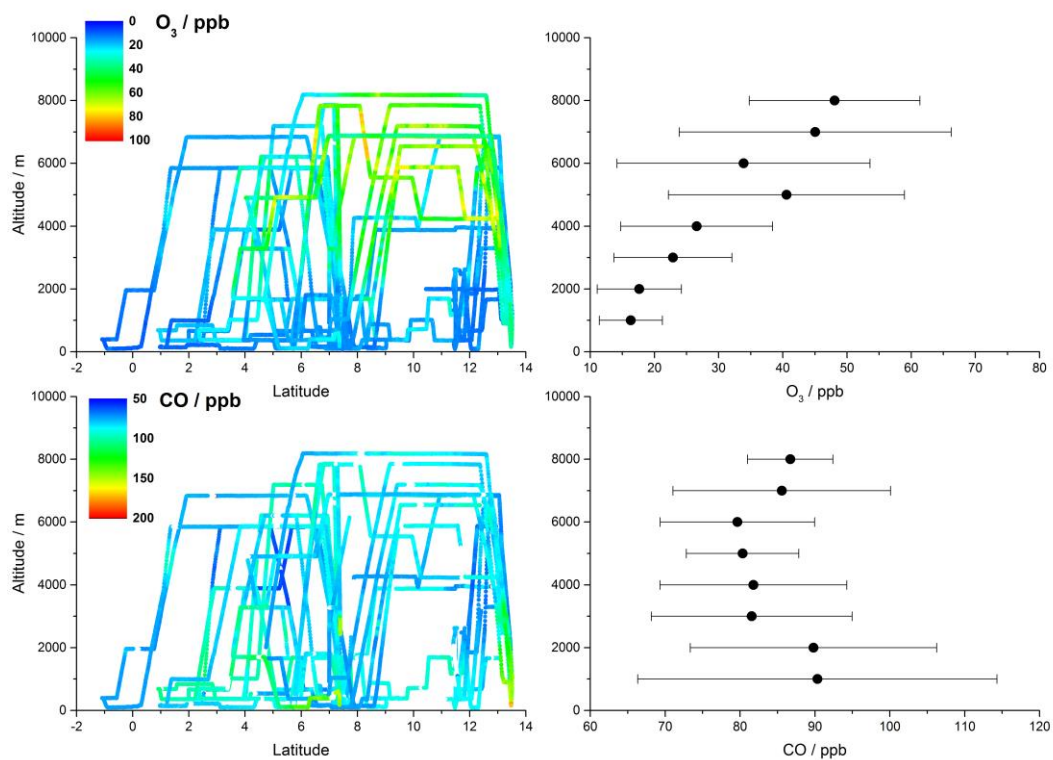
736

737 Figure 2: Map of FAAM BAe-146 flight tracks during January and February 2014. The flights
738 tracks are coloured by altitude. The islands of Guam, Palau and Chuuk are marked. The
739 background shows Jan-Feb averaged Chlorophyll-a concentrations, measured by the
740 MODIS satellite (NASA Giovanni, Acker et al., 2007). The inset shows an enlarged
741 area around Chuuk Atoll.

742

743

744



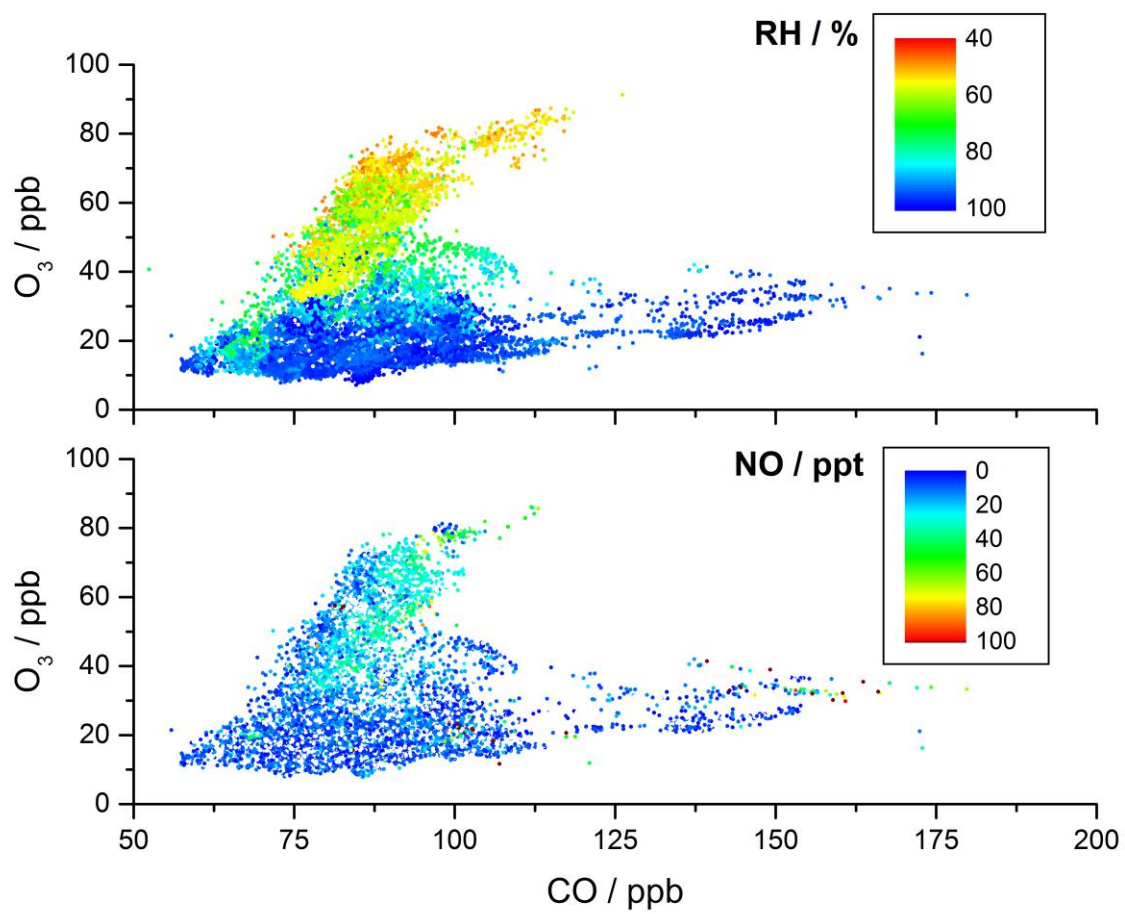
745

746 Figure 3: Ozone and carbon monoxide mixing ratios measured in all CAST flights as a function
747 of latitude and altitude (left). The means and associated 2 standard deviations of ozone
748 and carbon monoxide are shown as a function of altitude (right). See text and Table 1
749 for instrumental details.

750

751

752



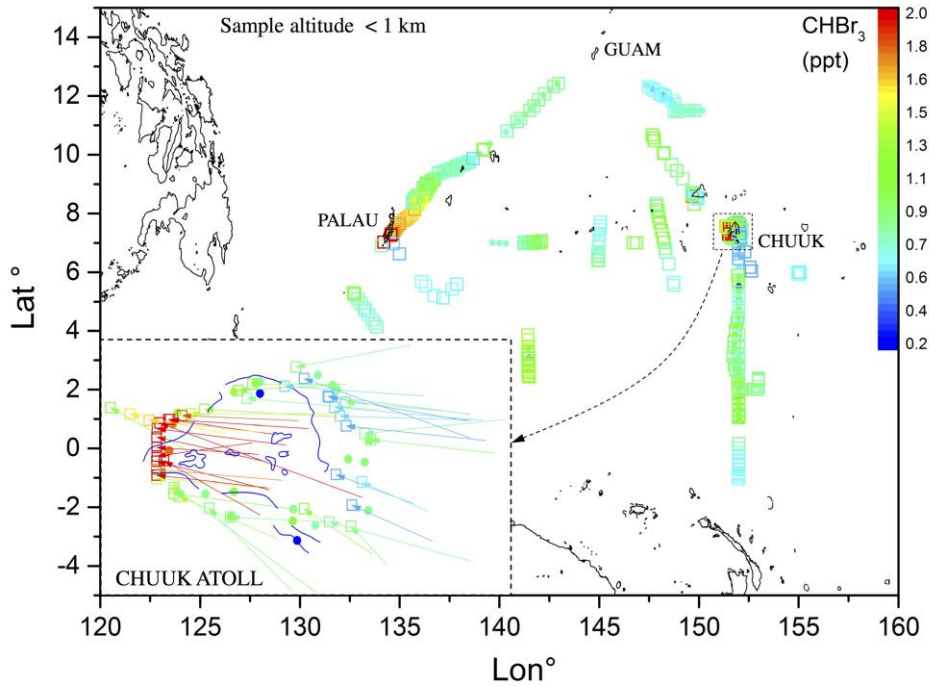
753

754

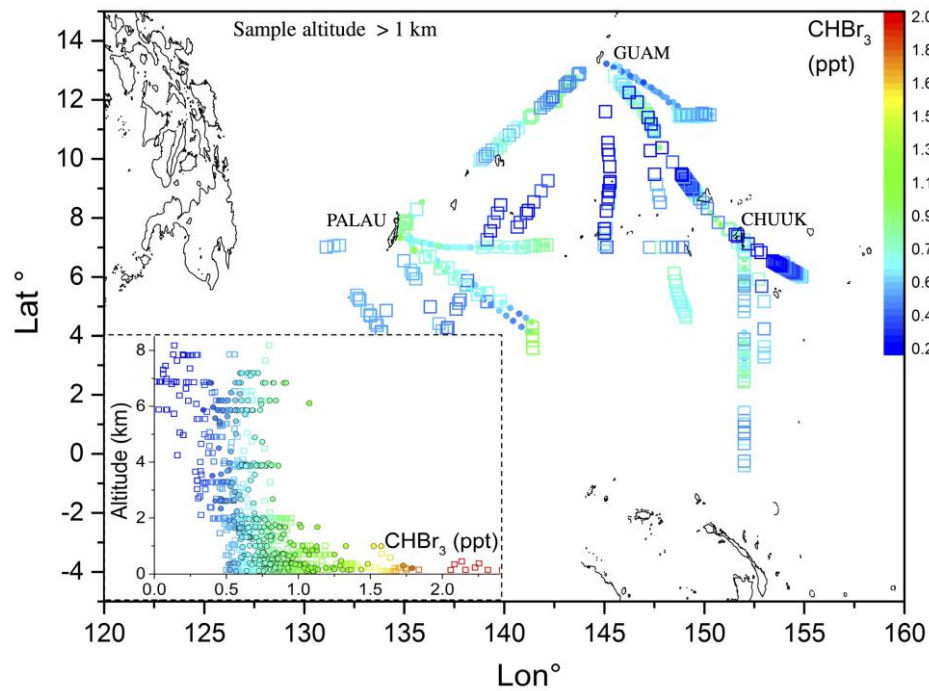
755 Figure 4: Plots of O_3 against CO coloured by (upper) NO and (lower) relative humidity (10 s
756 averaged data).

757

758



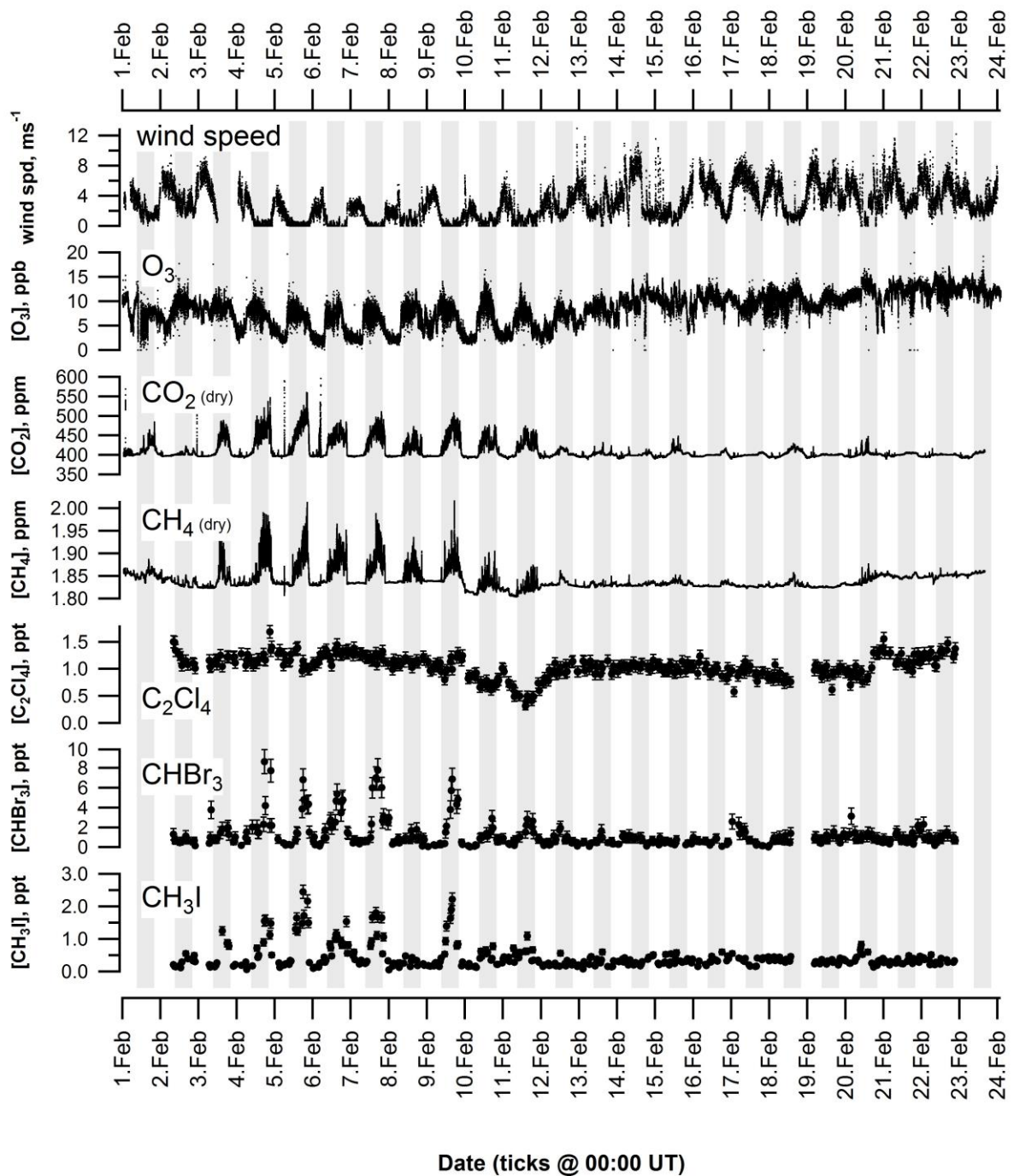
759



760

761

762 Figure 5: CHBr₃ mixing ratios (colours) sampled on the FAAM aircraft during CAST using the
763 whole air sampler (squares) and the on-board GC-MS (circles). Panel (a) contains all
764 measurements made at altitudes less than 1 km, and the enlarged inset (bottom left)
765 shows the values around the Chuuk Atoll. The lines associated with each measurement
766 in the inset indicate the instantaneous wind speed measured by the aircraft. Panel (b)
767 contains the measurements at altitudes greater than 1 km, and the inset shows the
768 vertical profile of all measurements.



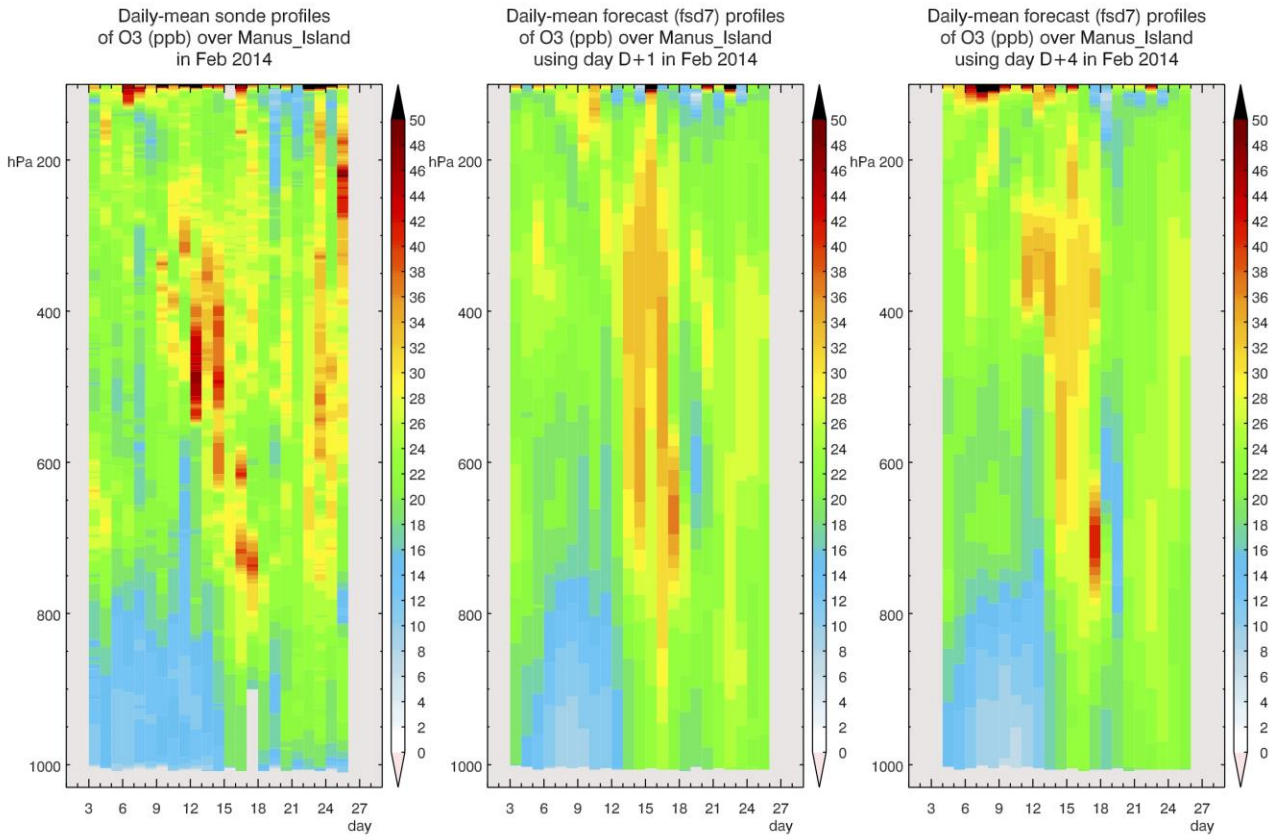
769
770

771

772 Figure 6: Surface observations of wind, O₃, CO₂, CH₄, C₂Cl₄, CHBr₃ and CH₃I at the ARM
773 Facility on Manus Island, Papua New Guinea (2.07°S, 147.4°E) from February 1-24,
774 2014. The time shown in the x-axis is Universal Time. The shading indicates the local
775 time, with the darker bands representing night-time.

776

777

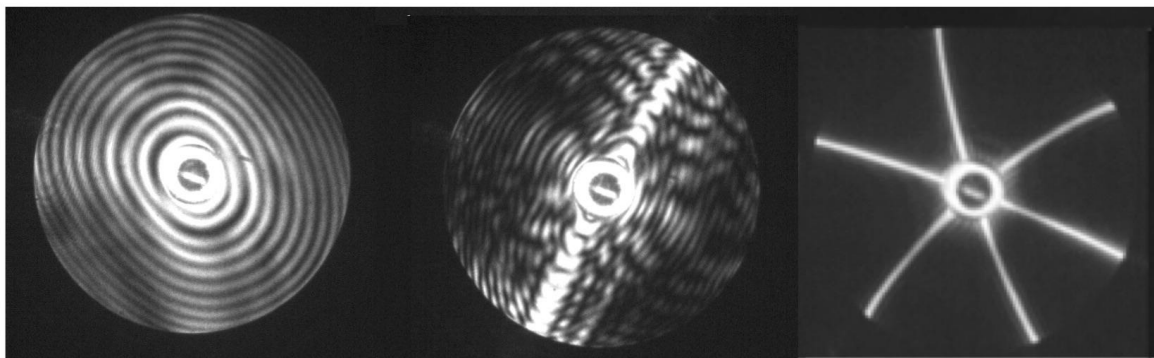


778

779 Figure 7: Daily observed ozone profile in Manus (left) and corresponding MACC forecast with a lead
780 time of 1 day (middle) and 4 days (right).

781

782



784

785

786

787

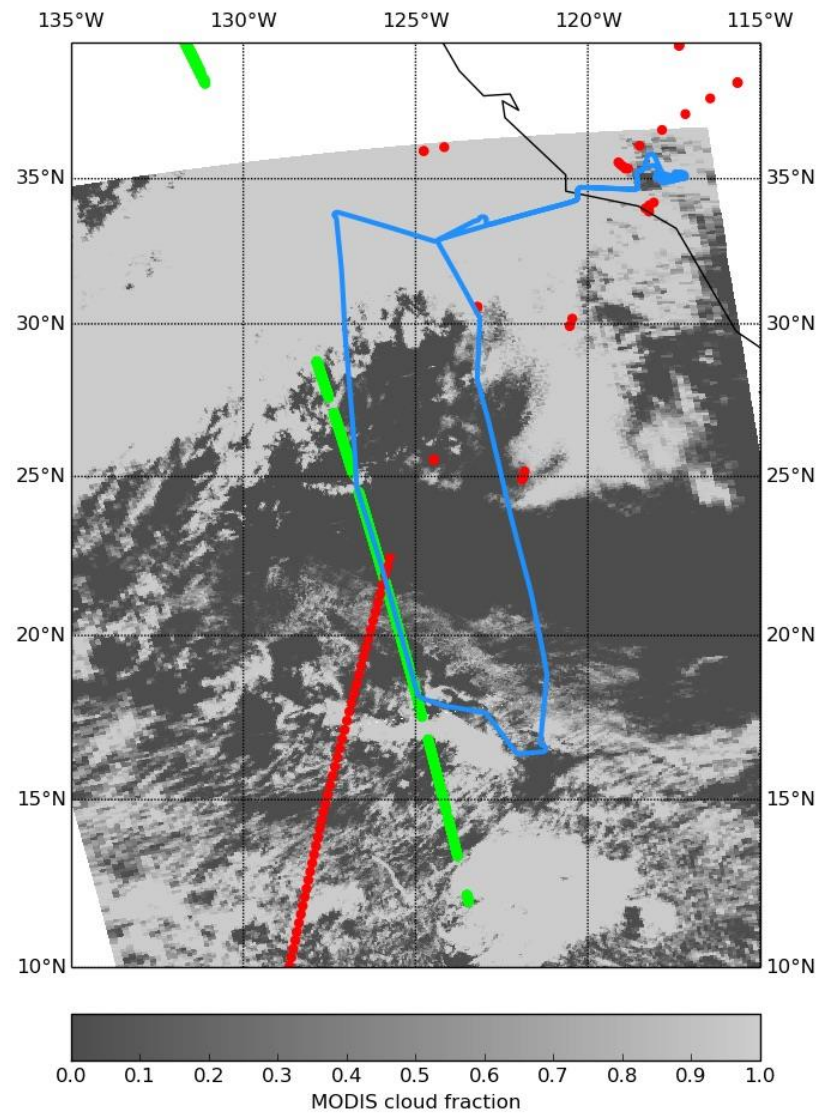
788

789

790

791

Figure 8: AIITS scattering patterns recorded from ice particles in the UTLS, at altitudes of ~ 16 km and temperatures of $\sim -80^{\circ}\text{C}$. The pictures are indicative of (left) a smooth quasi-spherical ice particle, (middle) a columnar crystal, and (right) a pristine hexagonal plate.



793

794

795 Figure 9: Flight path of the NASA Global Hawk on 10th March 2015 (blue). OCO-2 (green) and
 796 GOSAT (red) soundings are shown which coincide temporally with the flight leg
 797 between 25°N, 127°W and 18°N, 125°W. MODIS cloud fraction data (Platnick et al.,
 798 2015) coincident with the OCO-2 overpass at 2140 UTC is plotted in grayscale,
 799 showing the largely cloud-free conditions encountered during this leg of the flight.

800

801